Travelling-wave Mach-Zehnder Modulator as a Temporal Integrator and a Time-gate Isolator

Binhuang Song, Leimeng Zhuang, *Senior Member*, *IEEE*, and Arthur J. Lowery, *Fellow*, *IEEE*

***Abstract*— This work demonstrates that a commercial travelling-wave Mach-Zehnder modulator is a versatile device. Next to being a modulator, it is also able to function as an electro-optical temporal integrator with an integration window twice as long as its propagation delay. Using the similar principle and being driven by a periodic RF frequency, the modulator is able to perform as an optical time-gate isolator that blocks any reverse-travelling lightwave, but simultaneously allows forward-travelling periodically-pulsed optical signals to pass. In the experiment, sub-nanosecond forward-travelling time gates and reverse-travelling optical power extinction > 20 dB are successfully demonstrated.**

***Index Terms*— Travelling-wave Mach-Zehnder modulator, Microwave photonics, Temporal integrator, Isolators.**

I. Introduction

INTEGRATING optical systems on miniaturized optical chips is the key to enabling precise manipulations of light and reducing cost [1]. However, the lack of practical integrated optical isolators impedes the development of complex active circuits on photonic integrated circuits (PICs). For example, optical feedback into a laser cavity may cause increased noises and even chaotic behaviours [2].

In a general sense, ideal optical isolators should only allow lightwaves to pass in one direction even when there are forward and backward waves as illustrated in Fig. 1a, regardless of wavelength, power, and polarization [3]. At present, on-chip isolators are mostly implemented using magneto-optic materials that enable non-reciprocal absorption or phase shift [4]. However, this approach has high insertion loss and its integration requires non-standard fabrication processes. Other approaches (pseudo isolators) based on phase modulator [5] and acousto-optic modulator [6] have drawbacks of complex circuit architecture and limited extinction ratio, which hinders their adoption for practical applications.

While implementing ideal optical isolators is still a challenge, some alternative approaches have been found promising for the implementation of the so-called time-gate isolators, i.e. devices providing time-gated transmission of lightwaves in one direction and constant isolation of lightwave in the reverse direction [7]. As shown in Fig. 1, such time-gate isolators are able to operate with periodically pulsed optical signals [8] that have applications in many different areas such as optical communications, LIDAR, spectroscopy, and optical clock distribution. The solution in [7] uses a 3-segment semiconductor optical amplifier. Such devices can be integrated into a small chip and can perform various functions (e.g. a time discriminator for optical pulses) [9]. However, this solution has a limited extinction ratio and it requires two electrical driving signals for the timing control.

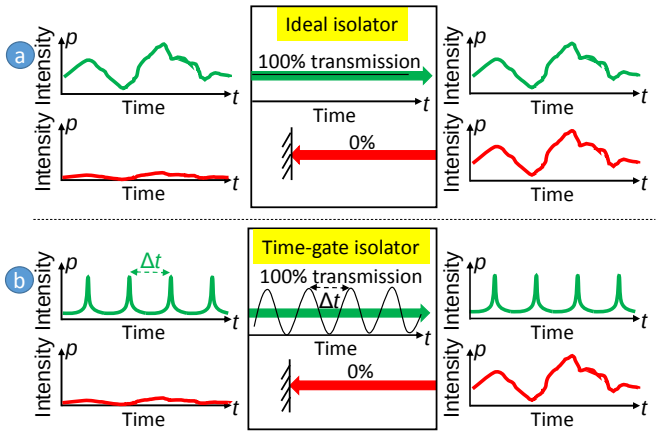

Fig. 1. Illustrations of: (a) an ideal isolator and (b) a time-gate isolator.

In this work, we show a simple implementation of a time-gate isolator using a commercial travelling-wave Mach-Zehnder modulator (TW-MZM) [10], an illustration of which is shown in Fig. 2. As a versatile device, a TW-MZM has been utilized for a number of electro-optical functions including nonreciprocal transmission in binary phase-shift keying modulation [11, 12] and all-optical DAC for pulse amplitude modulation [13]. Here, we experimentally demonstrate that a TW-MZM is able to function as an electro-optical temporal integrator and its bias provides a degree of freedom for controlling the DC component in the optical output. Utilizing these capabilities and being driven by a periodic RF signal, the TW-MZM is able to act as a time-gate optical isolator that blocks any reverse-travelling lightwave, but it simultaneously allows forward-travelling periodically-pulsed optical signals to pass. This particular function is implemented using the unique co-propagation (lightwave travels forward through the modulator with the electrical signal) and counter-propagation

This work is supported under the Australian Research Council's Laureate Fellowship (FL130100041) and CUDOS – ARC Centre of Excellence for Ultrahigh bandwidth Devices for Optical Systems (CE110001018).

Binhuang Song, Leimeng Zhuang and Arthur J. Lowery are with the Department of Electrical and Computer Systems Engineering, Monash University, Melbourne, VIC 3800, Australia (e-mail: binhuang.song@monash.edu;leimeng.zhuang@monash.edu;arthur.lowery@monash.edu).

(lightwave travels reverse through the modulator against the electrical signal) interactions of optical and electrical signals in the modulator [10]. Unlike the regular modulation operation using only co-propagation, counter-propagation yields a modulator output equal to a temporally integrated version of the input electrical signal, with an integration window twice as long as the propagation delay of the modulator [13]. As illustrated in Fig. 2b, when the input electrical signal is a periodic RF frequency and the integration window is an integer multiple of its period, the outcome of the integration is constant zero, or in other words, the input RF signal has no impact on the modulator output for a reverse-travelling lightwave. This means that when the modulator is biased at zero-transmission, it blocks any reverse-travelling lightwave independent of the phase of the modulating wave, as long as the modulating frequency is carefully chosen. In contrast, the forward-travelling lightwave is subject to a regular modulation operation driven by the RF signal. As such, every RF signal peak in a sinusoidal period drives the modulator away from the zero-transmission status and in effect opens a transmission time gate for the forward-travelling lightwave.

II. Device Working Principle

Assuming that the modulator has a negligible polarization-dependency and has a modulation section between positions 'd_i' and 'd_{ii}' with a time delay of $\Delta\tau$, as illustrated in Fig. 2a, then

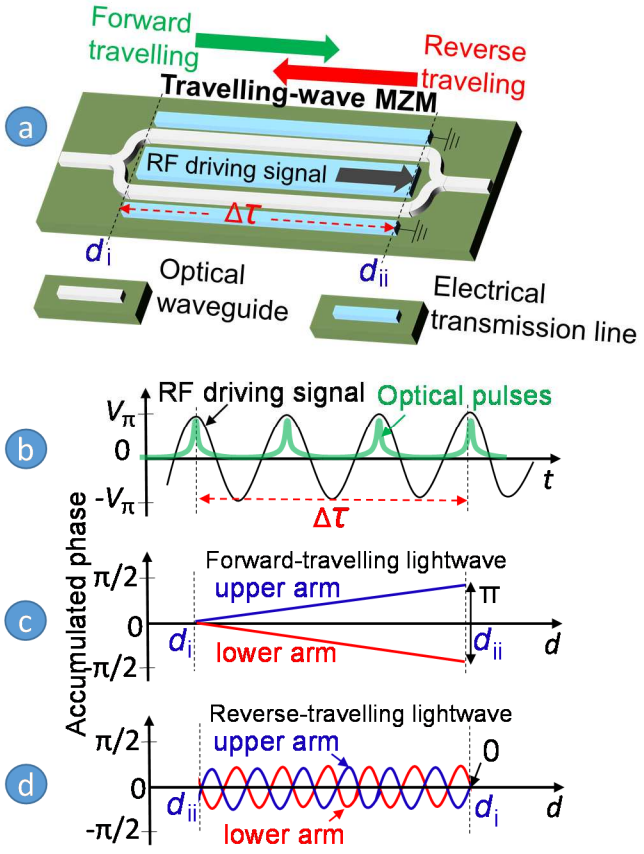

Fig. 2. (a) A schematic of a TW-MZM. (b) An illustration of a RF driving signal time-aligned with optical pulses. Position-domain illustrations of the accumulated phase modulation of (c) the forward-travelling lightwave and (d) reverse-travelling lightwave.

the accumulated inter-arm phase difference of the forward-travelling lightwave, $\Delta\theta(t)$, (illustrated in Fig. 2c) is given by

$$\Delta\theta(t) = \theta_{up}(t) - \theta_{low}(t) = 2\theta_{up}(t)$$
$$= \frac{\pi V_{RF}}{\Delta\tau V_\pi}\int_0^{\Delta\tau} \alpha(\tau)\cos(2\pi f_{RF} t)d\tau - \theta_{Bias} \quad (1)$$

where: θ_{up} and θ_{low} are the accumulated phase shifts of the upper and lower arms, respectively, with θ_{up} = - θ_{low} due to the push-pull configuration; V_π is the modulator RF half-wave voltage; V_{RF} and f_{RF} are the RF driving signal peak voltage and frequency, respectively; $\alpha(\tau)$ is the amplitude transmission coefficient of the RF signal when travelling along the modulator that is determined by the propagation loss of the RF electrode, θ_{Bias} is the modulator DC-bias phase shift. This equation shows that when the modulator satisfies the following conditions, namely zero-transmission bias with $\theta_{Bias} = \pi$, $V_{RF} = V_\pi$, and negligible RF propagation loss with $\alpha(\tau) = 1$, $\Delta\theta(t)$ will swing between -π and π (equivalent to 0 and -2π) in accordance with the RF driving signal, providing periodic chirp-free transmission with preserved polarity (when $0 \le \Delta\theta(t) < \pi$). These transmission window allow periodically-pulsed optical signals to pass, assuming the pulse width is much narrower than that of the time gate window. The pulse shape impairment due to an amplitude modulation, $\cos(\Delta\theta(t))$, can be minimized by time-aligning the optical and RF signal peaks, e.g. using a pulse interval of Δt, $f_{RF} = 1/\Delta t$.

In contrast, as explained in [13], the reverse-travelling lightwave undergoes oscillations of phase modualtion. Its accumulated inter-arm phase difference, $\Delta\theta'(t)$, is illustrated in Fig. 2d, whose mathematical expression is given by

$$\Delta\theta'(t) = \frac{\pi V_{RF}}{\Delta\tau V_\pi}\int_0^{2\Delta\tau} \alpha(t/2)\cos(2\pi f_{RF} t)dt - \theta_{Bias}. \quad (2)$$

It can be derived that assuming the RF electrode has negligible loss with $\alpha(t/2) = 1$ and $f_{RF} = n/(2\Delta\tau)$ with n is an integer, the integration evaluates to zero. With this condition satisfied and modulator biased at zero-transmission ($\theta_{Bias} = \pi$), the reverse-travelling lightwave will be significantly suppressed regardless of timing and waveform. It should be mentioned that for the optimal performance of the operations in Eq. (1) and (2), a implementation of the modulator is needed that not only features a RF electronde with low propagation loss and propagation velocity matching to the optical waveguide [14], but also a high optical power extinction ratio between the minimum- and maximum-transmission biases. This poses a challenge for the device design, particularly for high-frequency operations, e.g. tens of GHz.

III. Experimental Demonstration

A. Modulator Characterization

For the experiment, we used a commercial 20-GHz TW-MZM (Covega). The modulator's amplitude modulation responses for both forward-travelling and reverse-travelling lightwave were first characterized, where the lightwave for the measurement was generated from a CW laser (Gooch &

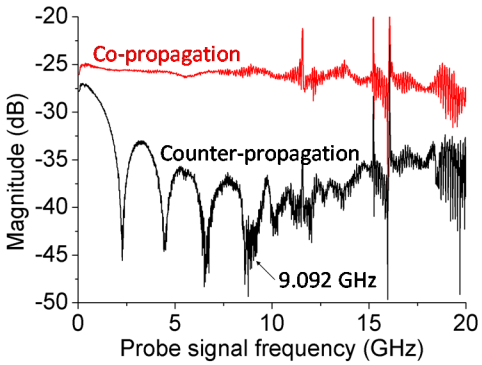

Fig. 3. Modulator frequency responses for counter- and co-propagating electrical and optical signals.

Housego AA0701) and the RF driving signal was generated using a vector network analyser (Anritsu 37247D). For both forward-travelling and reverse-travelling cases, the modulator output was detected by an 18-GHz DC-coupled RF photodetector (Discovery DSC-40S), which fed the detected RF signals back to the vector network analyser to determine the S_{21} parameter. Fig. 3 plots the measured RF frequency responses. In the reverse-travelling case, the nulls in the S_{21} response indicate the frequencies with which the integration outcome of Eq. (2) equals zero. The propagation delay of the modulator can be derived from the first null, f_1 = 2.273 GHz, by $\Delta\tau = 1/(2f_1)$= 220 ps. The additional loss of the reverse-travelling case at low frequencies results from a polarization misalignment.

B. *Demonstration of Analog Temporal Integrator*

To demonstrate the electro-optical temporal integrator function of the modulator, a CW lightwave was fed into the modulator in the reverse-travelling direction and several types of electrical pulses were applied as the modulator driving signal (Tektronix AWG7102). Figure 4a to 4c show the electrical pulses applied to the modulator, in which '4a' is a single pulse with a pulse width of 100 ps, '4b' is formed by two such pulses with a time interval of 50 ps, and '4c' comprises two such pulses with a time interval of 300 ps. The corresponding output optical powers are shown in Fig. 4d to 4f. It is clear that the modulator works as a temporal integrator. For a single electrical input pulse (Fig. 4a and 4b), the modulator output shows a gate-like waveform whose amplitude varies in accordance to the peak amplitude of the electrical input pulse. The width of the gate is about 600 ps, which results from the integration window of the modulator, $2\Delta\tau$ = 440 ps, and width of the electrical pulse. For the electrical input of two sequential pulses (Fig. 4c), the waveform that has two sequential steps is observed in the output, with the steps coinciding with the peaks of the two electrical pulses. The down-step in the modulator output indicates the end of the integration window to each electrical input pulse. It is worth mentioning that next to enabling the time-gate isolator function discussed in this work, such an electro-optical temporal integrator also has potential for other functions, e.g. a logic adder for the generation of control signals or an analog signal processor in microwave photonics [15, 16].

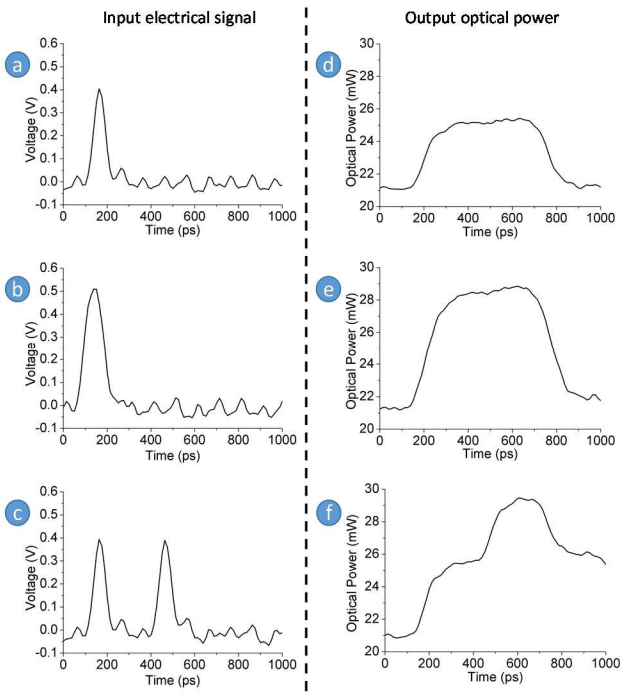

Fig. 4. (a–c) Input RF signals to the modulator, (d–f) corresponding output optical power of the modulator.

C. *Demonstration of Time-gate Isolator*

To demonstrate the time-gate isolator function, we biased the modulator at zero-transmission ($\theta_{Bias} = \pi$) which corresponds to a modulator power extinction ratio of 21.5 dB. An input RF tone with a frequency f_{RF} = 9.092 GHz is applied as the driving signal, i.e. the 4th null of the S_{21} for reverse-travelling lightwave in Fig. 3. The forward-travelling optical signal was a periodic pulse train with a pulse width of about 50 ps and a pulse interval $\Delta t = 4\Delta\tau$ = 1.76 ns. The optical pulses were generated by directly modulating a CW laser (Gooch & Housego AA0701) with an electrical pulse train from a bit pattern generator (SHF BPG 44E), which used the same clock signal as the RF driving signal source to guarantee signal synchronization. As shown in Fig. 5a, the pulse-train peaks were time-aligned with the amplitude peaks of the RF driving signal to maximize the transmission when the gate is open. Fig. 5b shows the output pulses in comparison with the case when the modulator is biased for maximum transmission ($\theta_{Bias} = 0$) without RF driving signals. This result demonstrates the expected transmission of the forward-travelling optical pulses. Although both cases have the same intrinsic modulator loss, the time-gated output is lower than that of the modulator's maximum transmission. This is

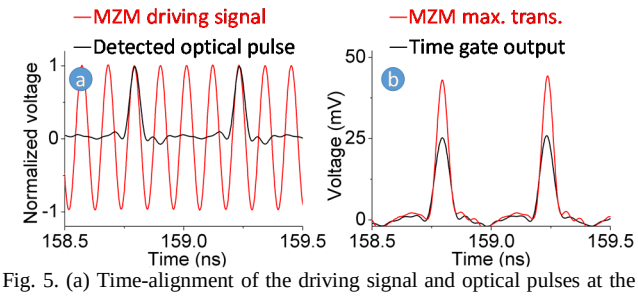

Fig. 5. (a) Time-alignment of the driving signal and optical pulses at the input of modulator; (b) detected time gate output pulses in comparison with the output when the modulator is biased at maximum transmission.

because the modulator driving signal's amplitude, V_{RF} = 2.5 V, was smaller than the modulator's on-off switching voltage, V_π = 4 V, resulting in the maximum time gate amplitude transmission < 1, i.e. $\max(\eta(t)) = \sin(\pi V_{RF}/2V_\pi) = 0.83$ (equivalent to a power factor of 0.69).

Time misalignment between the modulator driving signal and optical pulses causes asymmetrical pulse waveform distortion. A demonstration of this effect is presented in Fig. 6.

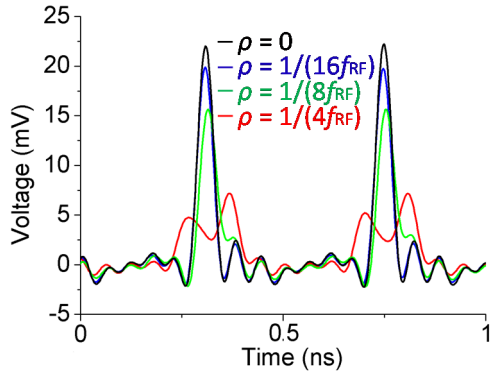

Fig. 6. Pulse distortion due to time misalignment between the RF driving signal and optical pulses.

When the time misalignment equals to a quarter of the RF driving signal period $\rho = 1/(4f_{RF})$, the optical pulses move from the peaks to the nulls of the transmission, resulting in pulse suppression and pulse splitting.

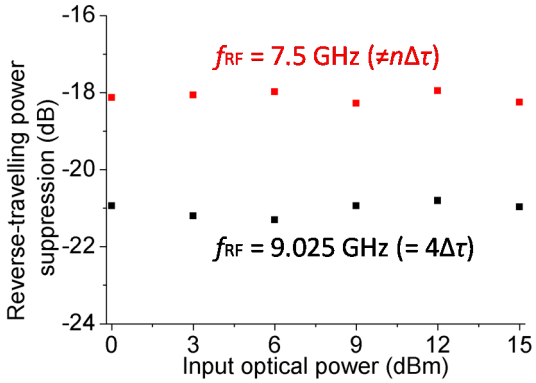

Fig. 7. Isolator reverse-travelling power suppression measurements for counter-propagating optical signals.

To demonstrate the blocking/isolation of the modulator to any reverse-travelling lightwave, a CW lightwave was applied to the modulator in the reverse-travelling direction to the RF driving signal. Fig. 7 shows the measured power suppression for different input CW powers. As expected, when the modulator is biased at zero-transmission and the RF driving signal satisfies $f_{RF} = n/(2\Delta\tau)$ (n = 4 in this experiment), the reverse-travelling power suppression is nearly the same as the modulator extinction ratio of 21.5 dB. This result verifies the operation explained in Eq. (2) and indicates a suitably low propagation loss of the RF electrode. However, when the condition of the RF driving signal frequency is broken, the integration operation in Eq. (2) evaluates to a non-zero value, which drives the modulator away from its zero-transmission bias status, and as a result reduces the reverse-travelling power suppression. It is worth mentioning that our implementation of the isolator is independent of input power, which would not be the case for isolators that rely on nonlinear-optical effects [17].

IV. Conclusion

Using a commercial TW-MZM, we have successfully demonstrated the versatile functions of an electro-optical temporal integrator and an optical time-gate isolator. The integrator function leverages the modulator's electrical bandwidth and provides an integration window twice as long as the propagation delay of the modulator. The time-gate isolator function supports a sub-nanosecond time-gate transmission to forward-travelling periodically pulsed optical signals and provides simultaneously >20-dB power extinction to any reverse-travelling lightwave. These functions show the versatile uses of TW-MZMs in electro-optical signal processing. Although the current demonstration is based on a commercial LN modulator, the same technique can be extended to silicon and InP on-chip MZMs, incorporating in complex on-chip systems with photonic integrated circuits.

References

[1] M. Smit, J. Van der Tol, M. Hill, "Moore's law in photonics," *Laser Photon. Rev*., vol. 6, no. 1, pp. 1-13, 2012.
[2] R. Tkach, A. Chraplyvy, "Regimes of feedback effects in 1.5μm distributed feedback lasers," *J. Lightwave Technol.*, vol. 4, no. 1, pp. 1655-1661, 1986.
[3] D. Jalas *et al.*," What is–and what is not–an optical isolator," *Nat. Photon.*, vol. 7, no. 8, pp. 579-582, 2013.
[4] Z. Yu and S. Fan, "Complete optical isolation created by indirect interband photonic transitions," *Nat. Photon.*, vol. 3, no. 2, pp. 91-94, 2009.
[5] C. Galland *et al.*, "Broadband on-chip optical non-reciprocity using phase modulators," *Opt. Exp*., vol. 21, no. 12, pp. 14500-14511, 2013.
[6] L. D. Tzuang *et al.*, "Non-reciprocal phase shift induced by an effective magnetic flux for light," *Nat. Photon.*, vol. 8, no. 9, pp. 701-705, 2014.
[7] M. J. R. Heck *et al*., "Integrated microwave photonic isolators: theory, experimental realization and application in a unidirectional ring mode-locked laser diode," *Photonics*, vol. 2, no. 3, pp. 957-968, 2015.
[8] A. Zheltikov, "Few-cycle laser pulse generation and its applications," in *Topics in Applied Physics*, Vol. 95, F. X. Kärtner Ed. New York, Springer, 2005, pp. 1088-1089.
[9] A. J. Lowery and L. Zhuang, "Photonic integrated circuit as a picosecond pulse timing discriminator," *Opt. Exp.*, vol. 24, no. 8, pp. 8776-8781, 2016.
[10] G. K. Gopalakrishnan *et al.*, "Performance and modelling of broadband $LiNbO_3$ travelling wave optical intensity modulators," *J. Lightwave Technol.*, vol. 12, no. 10, pp. 1807-1819, 1994.
[11] P. Dong, "Travelling-wave Mach-Zehnder modulators functioning as optical isolators," *Opt. Exp*., vol. 23, no. 8, pp. 10498-10505, 2015.
[12] P. Dong and C. Gui, "Observation of nonreciprocal transmission in binary phase-shift keying modulation using traveling-wave Mach-Zehnder modulators," *Opt. Lett*., vol. 41, no. 12, pp. 2723-2726, 2016.
[13] A. J. Lowery, "All-optical DAC using counter-propagating optical and electrical pulses in a Mach-Zehnder modulator," *Opt. Exp*., vol. 22, no. 21, pp. 26429-26437, 2014.
[14] E. Wooten *et al.*, "A review of lithium niobate modulators for fiber-optic communications systems." *IEEE J. Sel. Topics Quantum Electron.*, vol. 6, no. 1, pp. 69-82, 2000.
[15] J. Zhang and J. Yao, "Microwave photonic integrator based on a multichannel fiber Bragg grating," *Opt. Lett*., vol. 41, no. 2, pp. 273-276, 2016.
[16] R. Slavík *et al.*, "Photonic temporal integrator for all-optical computing," *Opt. Exp*., vol. 16, no. 22, pp. 18202-18214, 2008.
[17] Y. Shi, Z. Yu, and S. Fan, "Limitations of nonlinear optical isolators due to dynamic reciprocity." *Nature photon.*, vol. 9, no. 6, pp. 388-392, 2015.